frontiers in Materials

ORIGINAL RESEARCH
published: 16 September 2021
doi: 10.3389/fmats.2021.720385

Production and Characterization of Keratin/Tragacanth Gum Nanohydrogels for Drug Delivery in Medical Textiles

Nazanin Mansouri Shirazi, Niloofar Eslahi and Adeleh Gholipour-Kanani*

Department of Textile Engineering, Science and Research Branch, Islamic Azad University, Tehran, Iran

Keratin protein has been applied for biomedical applications due to its biocompatibility, biodegradability, mechanical resistance, and bioavailability. Tragacanth gum (TG) as a polysaccharide-based biopolymer has wound healing and antimicrobial properties. In this study, keratin was extracted from protein-based chicken feather by using reduction hydrolysis (sodium sulfide), and nanogels of keratin and TG composites at different ratios were produced by using the chemical cross-linking method. Then, cinnamon (5 and 10%) as an antibacterial herbal extract was added to the nanogels and coated on cotton fabric. The morphology and size of the composite nanogels, chemical structure, biological, and antibacterial properties were evaluated. According to DLS results, TGK2:1 (ratio of TG to keratin = 2:1) had the minimum size (80 nm) and PDI (0.1), and therefore, this sample was chosen as the optimum one. FESEM and TEM images showed the semi-spherical shape of the produced nanogels. FTIR spectra revealed the possible hydrogen bonding between the components, and the formation of disulfide bonds after the addition of hydrogen peroxide was confirmed by XPS. After loading cinnamon into the nanogels, an increase in size was observed from 80 nm for free-nanogel to 85 and 105 nm for 5 and 10% extract-loaded nanogels, respectively. Besides, more cinnamon was released from the treated fabrics by increasing time and cinnamon concentration. The antibacterial test exhibited good antibacterial properties against both Gram-positive and Gram-negative bacteria. Finally, MTT assay approved the biocompatibility of the produced nanogels for potential use in medical textiles.

Keywords: keratin, tragacanth gum, nanogel, drug delivery, medical textiles

OPEN ACCESS

Edited by:
Nafisa Gull,
University of the Punjab, Pakistan

Reviewed by:
Sharjeel Abid,
National Textile University, Pakistan
Hossam Elsayed Emam,
National Research Centre, Egypt

****Correspondence:***
Niloofar Eslahi
niloofar.eslahi@srbiau.ac.ir

Specialty section:
This article was submitted to Polymeric and Composite Materials, a section of the journal Frontiers in Materials

Received: *04 June 2021*
Accepted: *23 August 2021*
Published: *16 September 2021*

Citation:
Mansouri Shirazi N, Eslahi N and Gholipour-Kanani A (2021) Production and Characterization of Keratin/Tragacanth Gum Nanohydrogels for Drug Delivery in Medical Textiles. Front. Mater. 8:720385. doi: 10.3389/fmats.2021.720385

INTRODUCTION

Hydrogels are hydrophilic three-dimensional networks that swell in contact with water but do not dissolve. They come in many forms, including sheets, microparticles, nanoparticles, coating structures, and films. For this reason, hydrogels can be used in diverse research areas including sensors, tissue engineering, and biomolecular separation (Amin et al., 2009). Nanogels or hydrogel nanoparticles are ideal candidates for target-specific delivery of drugs due to their high drug loading capacity, biocompatibility, biodegradability, and improved cellular uptake efficiency (Chacko et al., 2012; Cheng et al., 2013; McKenzie et al., 2015). Nanogels could be used as drug delivery vehicles capable of protecting the encapsulated drugs from the physiological environment and releasing them in the targeted tissues with meliorated permeability and retention effect (Sun et al., 2017).

Keratin is a natural protein with a cysteine-rich structure. It is found in different sources such as human hair, wool, feathers, horns, and nails and produced in various forms such as film, sponge, powder, and hydrogel. Bird feathers, as one of the important sources of keratin having disulfide bonds, hydrogen bonds, and hydrophobic interactions, can be used in biomedical applications (Eslahi et al., 2013). In addition, due to the presence of various functional groups, such as carboxyl, amid, or sulfhydryl, keratin could be easily modified with biomolecules to enhance its stability, solubility, as well as biocompatibility for drug carrier applications (Cilurzo et al., 2013). For instance, Li et al. (2012) synthesized keratin-g-PEG copolymers with dual triggerable release properties for cancer therapy. Cheng et al. (2018) studied keratin nanoparticles for controlled mucoadhesion and drug release. In another study, Sun et al. (2017) produced stimuli-responsive keratin-alginate nanogels as a drug carrier for doxorubicin hydrochloride (DOX). Zhang & Lui (2019) also investigated keratin-based nanoparticles for tumor intracellular DOX delivery. The results showed pH and reduction of dual-triggered drug release with enhanced antitumor efficacy.

In recent years, tragacanth gum (TG) has been used as a superabsorbent hydrogel, antimicrobial nanocapsules, wound dressings, skin scaffolds, and drug release systems (Meghdadi & Boddohi 2019; Zare et al., 2019). Tragacanth gum is a natural polysaccharide obtained from different species of *Astragalus* plant. This polysaccharide comprises an insoluble but a water-swellable fraction called bassorin and a water-soluble fraction called tragacanthin. In addition, the active ingredients in TG help to produce collagen and improve wound healing (Ghayempour et al., 2016). Pathania et al. (2018) fabricated TG nanohydrogels using microwave radiations for the controlled release of ampicillin. Besides, Verma et al. (2020) evaluated TG-lecithin core-shell nanogels by nanoemulsion process, in which cisplatin was encapsulated into the TG core of the nanogels.

Cinnamon is a natural preservative and flavoring material, which can be used as an interesting substitute for other chemical preservatives. Literature review showed that cinnamon can inhibit the growth of molds, yeasts, and bacteria (Matan et al., 2006). Cinnamon extract (CE) has diverse biological functions including antimicrobial, anti-inflammation, antioxidant, antidiabetic, and antitumor activity (Kwon et al., 2010). In spite of the significant antibacterial activity of CE, it is highly unstable and volatile. To overcome this issue, CE is encapsulated in composite hydrogels as promising long-term antibacterial materials with a sustained release profile. It is worth mentioning that although essential oils are prominent inhibitors of microorganisms, there is a limitation in their application due to their uncontrollable release. Some approaches such as designing mesoporous composites have been performed for the controlled release of essential oils (Abdelhameed at al. 2021).

Promoting the textile properties in different fields such as protective textile is of an interest and has been progressively considered especially in medical textiles. Recently, a novel technique has been reported by Emam et al. (2020) in which multifunctional textiles were prepared *via* incorporation of silicate and zeolitic imidazole frameworks on cotton fabric with durable protective activity against solar radiation as well as microbial pathogens.

The main goal of this research is to improve the drug-releasing property of textiles with the help of smart nanohydrogels. Despite several studies on keratin and polysaccharides, the fabrication of keratinpolysaccharide nanogels is still a challenge owing to the long molecular chains and strong hydrophilic interactions involved, which result in troubles in the formation of uniform-sized nanoparticles. To the best of our knowledge, the production of keratin and TG composite nanogels has not been reported yet. In this study, keratin was extracted from protein-based chicken feather by using reduction hydrolysis, and nanogel of keratin and TG was produced by using the chemical cross-linking method. Then, cinnamon as an antibacterial herbal extract was added to the nanogels, and the loaded nanogels were padded onto the cotton fabric. Finally, the fabricated composite hydrogels were tested by different analyses.

MATERIALS AND METHODS

Materials

White broiler chicken feathers were provided by a slaughterhouse in Iran. TG and cinnamon extract were supplied by the domestic market and Morvarid Farm Co. (Iran), respectively. Other chemicals such as sodium sulfide and hydrogen peroxide were of analytical grade and obtained from Merck Co., (Germany). 100% cotton fabric (145 g/m2) was also utilized as the textile substrate.

Extraction of Keratin

At first, feathers were washed with 1 g/L nonionic detergent and 1% sodium carbonate at liquid-to-goods ratio (L:G) of 40:1at 60°C for 30 min. Afterwards, they were treated with 80% methanol for 2 h to remove grease, then dried, and cut to 2–5 mm. Keratin was extracted from the cleaned feathers by using 10 g/L sodium sulfide for 3 h at 60°C (L:G = 30:1). After filtration, the keratin solution was dialyzed against distilled water with a cellulose tube (molecular weight cutoff = 3.5 KD) for 48 h with frequent water replacement. The purified keratin solution was concentrated by a rotary evaporator and finally freeze-dried to get feather keratin powder.

Fabrication of Composite Nanohydrogels

The produced keratin powder was mixed with TG in 40 ml distilled water under N_2 atmosphere at different mass ratios of 1:1, 1:2, and 2:1 (TG: keratin) for 1 h. Hydrogen peroxide (2 ml) was then added to the mixtures drop by drop to induce chemical cross-linking, and the mixtures were stirred for 24 h at 37°C. Then, the samples were dialyzed against distilled water for 48 h to remove excess H_2O_2 and finally freeze-dried.

CE Loading Into Nanohydrogels and Coating on Cotton Fabric

After determining the optimum ratio of the components, two different amounts of CE (5 and 10%) as an antibacterial herbal extract were added to the blend of TG and keratin before chemical

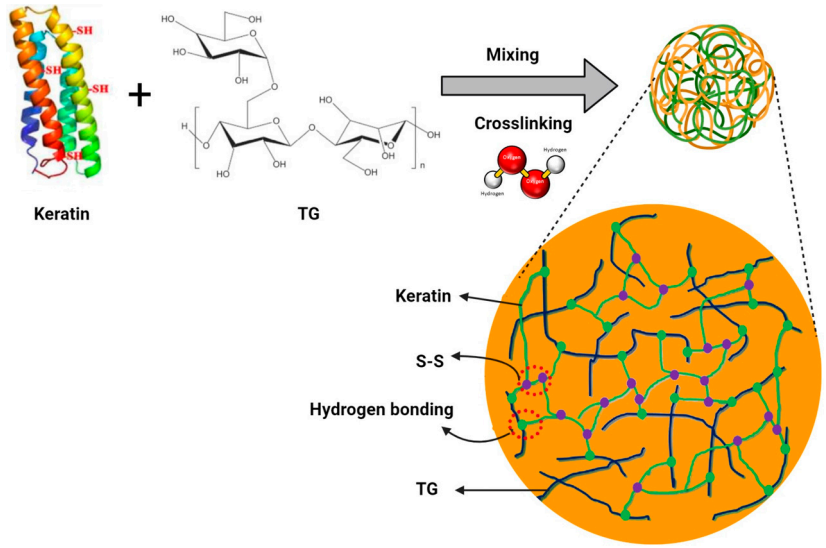

SCHEME 1 | Schematic illustration of TGK nanogels synthesized by chemical cross-linking.

cross-linking. The rest of steps were done according to the same procedure for the fabrication of composite nanogels. The supernatant was characterized *via* absorption spectra by UVVis spectroscopy (DR 5000™ UVVis Spectrophotometer, United States) at λ = 674 nm. CE loading content (CL) and encapsulation efficiency (E) of the nanogels were calculated by using the following equations:

$$CL = W_{CE.L}/W_{CE.TGK} \times 100 \quad (1)$$

$$E = W_{CE.L}/W_{CE.F} \times 100 \quad (2)$$

where $W_{CE.L}$, $W_{CE.TGK}$, and $W_{CE.F}$ are the weight of CE in the nanogels, the total weight of CE-loaded TGK nanogels, and the weight of feeding CE, respectively (Sun et al., 2018). Finally, the cotton fabrics (5 × 5 cm) were immersed in the prepared CE-loaded nanogels for 24 h and then dried in open air.

Characterization of Nanohydrogels

Physicochemical Properties

Morphological investigation of the prepared nanohydrogels was performed by field emission scanning electron microscopy (FESEM, Zeiss EM900, Germany) at an acceleration voltage of 20 kV as well as TEM (Zeiss, EM10C, Germany) at 100 kV. The size distribution and zeta potential of the nanoparticles were examined by dynamic light scattering (ZEN3600, Malvern, United Kingdom). For this test, the samples were dispersed in PBS (1 mg/ml) and sonicated with Ultrasonic Homogenizer (Misonix, S3000) at 20 kHz for 10 min. The chemical structure of the nanohydrogels was also investigated by Fourier transform infrared spectroscopy (FTIR, Thermo Nicolet Nexus 870, United States) using KBr pellets in the wavenumber range of 4,000–400 cm^{-1}. XPS was performed using an X-ray photoelectron spectrometer (Bes Tec, Germany) with Al Kα X-ray source (1,486.6 eV), and high-resolution binding energy regions for carbon (C1s) and sulfur (S2p) were investigated.

Release Study

To study the release percentage of the CE from the treated fabrics, the samples (3 × 3 cm) were precisely cut and then immersed in PBS (pH 7.4). At certain time intervals (0.5, 1, 2, 4, 8, 12, 24, 48, 72, 96, 120, 144, 168, 192 h), the incubation medium (2 ml) was removed and replaced with fresh PBS. This procedure was repeated twice. The amount of released cinnamon was then quantified by UVVis spectroscopy (DR 5000™ UVVis Spectrophotometer, United States) at λ = 674 nm.

Antibacterial Test

The antimicrobial activity of the CE-loaded nanohydrogel was assessed by agar well diffusion method. For this purpose, bacteria were transported to Mueller Hinton Broth medium and put in an incubator at 37°C for 3 h to obtain 0.5 McFarland. Then, 500 ml suspension of 1.5 × 108 CFU/ml was transported to Mueller Hinton agar and cultured. Then, a hole with a diameter of 6–8 mm was punched aseptically with a sterile cork bore, and a volume (100 µl) of the nanogel was introduced into the well and incubated at 37°C. The antimicrobial agent diffused in the agar medium and inhibited the growth of the microbial strain tested. Finally, the zone of inhibition was calculated after 24 h where bacteria growth is inhibited (Debalke et al., 2018).

In vitro Assay

The biocompatibility of free and CE-loaded nanogels was assessed using the 3-(4,5-dimethylthiazol-2-yl)-2,5-diphenylte-trazolium bromide (MTT) method. L929 fibroblast cells were cultured in

TABLE 1 | Average size and PDI of different samples.

Sample codes	Size (nm)	PDI
TGK11	88	0.521
TGK12	171	0.509
TGK21	80	0.100

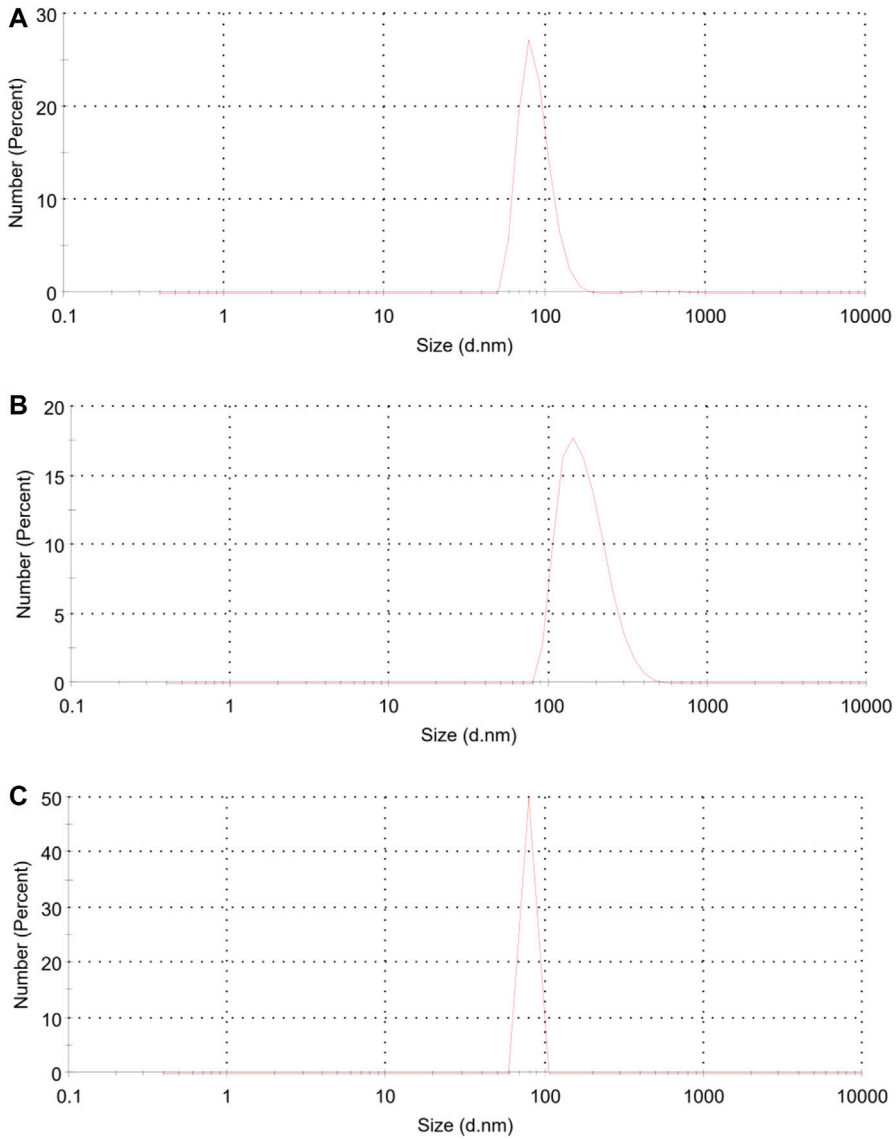

FIGURE 1 | Particle size distribution of different formulations: **(A)** TGK11, **(B)** TGK12, **(C)** TGK21.

RPMI-1640 medium containing 10% FBS, 50 U/ml penicillin, and 50 U/ml streptomycin and kept for 24 h at 37°C in a 5% CO2 humidified sterile incubator. After incubation at different times, 20 µl of 5 mg/ml MTT solution was added to each well containing the sample. Then, the MTT solution was replaced with 150 µl dimethyl sulfoxide (DMSO) and shacked for 10 min. Finally, the optical density of each well was measured at 570 nm using ELISA reader at 24, 48, and 72 h. Cell viability percentage was calculated in comparison to control sample by using the following equations:

$$\text{Toxicity } \% = \left(1 - \frac{\text{mean OD of sample}}{\text{mean OD of control}}\right) \times 100 \quad (3)$$

$$\text{Viability } \% = 100 - \text{Toxicity } \% \quad (4)$$

RESULTS AND DISCUSSION

Characterization of TG-Keratin Composite Nanohydrogels

TG-keratin composite nanohydrogels were synthesized in an aqueous solution *via* an oxidative cross-linking reaction with H_2O_2 (**Scheme 1**). The hydroxyl, carboxyl, and amino groups on keratin could form hydrogen bonds with carboxyl and hydroxyl groups on TG. After the addition of hydrogen peroxide, the thiol groups (-SH) of keratin were oxidized to form disulfide bonds, leading to keratin chain assembled, and TGK nanogels were consequently obtained. A similar mechanism was reported by Sun et al. (2018) for the formation of keratin and hyaluronan nanogels.

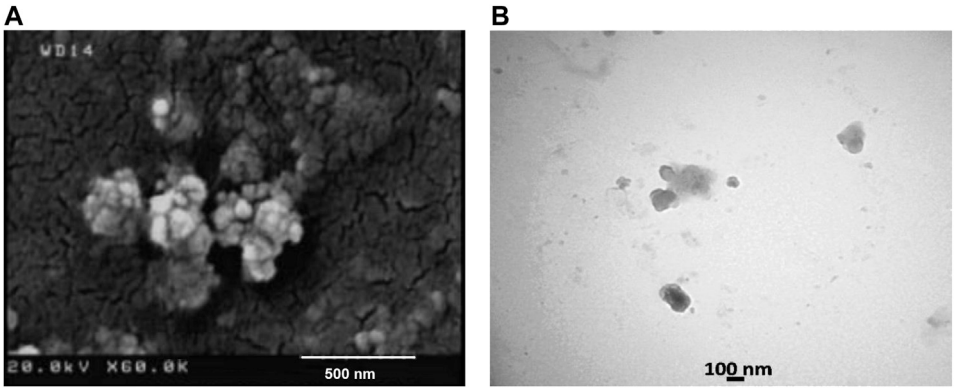

FIGURE 2 | (A): FESEM and **(B)**: TEM images of TGK21.

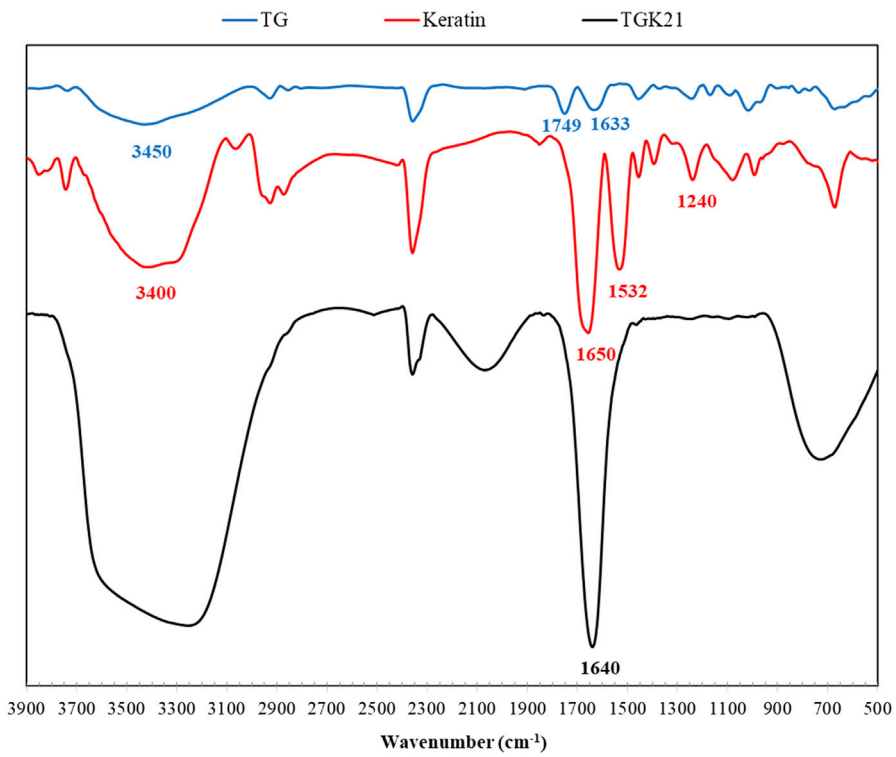

FIGURE 3 | FTIR spectra of keratin, TG, and TGK composite.

Size and Morphological Investigation

The average size as well as polydispersity index (PDI) of different formulations was measured by dynamic light scattering (DLS). **Table 1** shows that the TGK2:1 (ratio of TG to keratin = 2:1) has the minimum size and PDI and therefore this sample is chosen as the optimum one. The greater the proportion of TG, the smaller the particle size. The measured zeta potential of the fabricated nanogel was −30.2 mV, indicating suitable colloidal stability due to electric repulsion. It was assumed that the negative charge of the nanogels could be associated with the hydroxyl and carboxyl groups of keratin and TG. **Figure 1** illustrates the particle size distribution of different nanogels. The sharp peaks in DLS graphs revealed the homogenous mono dispersion of the samples. FESEM and TEM images (**Figure 2**) also depict the semi-spherical morphology of the produced nanoparticles, validating the results of DLS.

FTIR Spectroscopy

The FTIR spectra of samples are depicted in **Figure 3**. The broad absorption band in the range of 3,100–3,700 cm^{-1} is associated with the stretching vibration of N–H and O–H bonds. The peaks around 2,900 cm^{-1} are attributed to C–H stretching modes of aliphatic

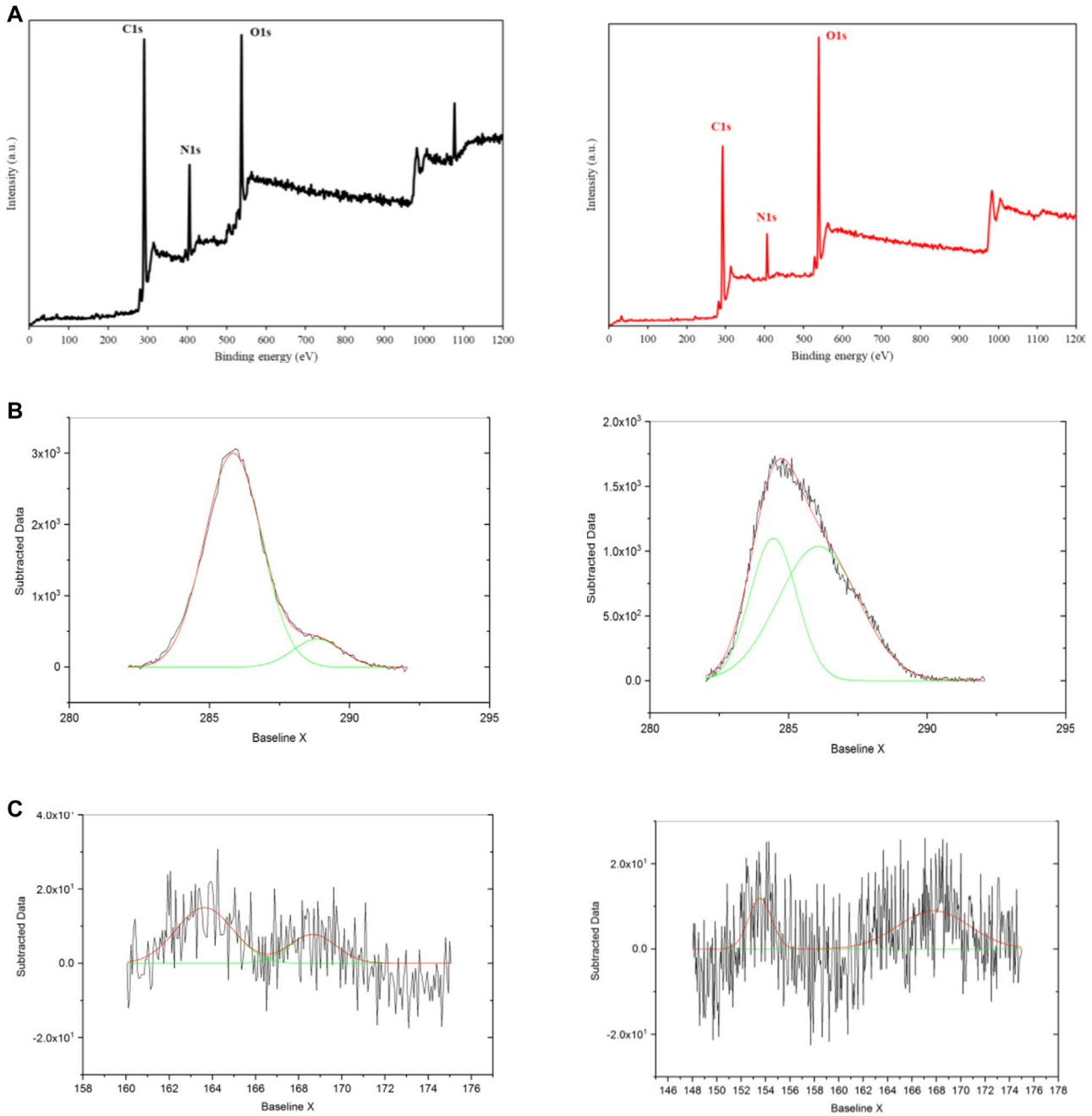

FIGURE 4 | XPS spectra of **(A)** whole regions, **(B)** C1s region, and **(C)** S2p region.

groups. As for keratin, the vibrations in the peptide bonds originate bands known as amide I, II, III. The amide I band in the range of 1700–1,600 cm^{-1} belongs to C=O stretching vibration, while the amide II appears at 1,532 cm^{-1} associated with N–H bending and C–H stretching vibration. The amide III band at 1,240 cm^{-1} is ascribed to C–N stretching and N–H in-plane bending (Eslahi et al., 2013). The spectrum of TG shows its characteristic peaks at 3,450 cm^{-1} (stretching vibration of hydroxyl groups), 2,925 cm^{-1} (the symmetric stretching of CH_2), 1749 cm^{-1} (carbonyl stretching vibration of galacturonic acid and its ester), 1,633 cm^{-1} (carboxylate stretching vibration of D-galacturonic acid), and 1,153 cm^{-1} (antisymmetric C-O-C vibrations of glycosidic groups of polysaccharides) (Fattahi et al., 2013; Singh and Sharma 2014). The FTIR spectrum of TGK composite exhibits the characteristic peaks of both TG and keratin with slight modification. For instance, the C=O stretching vibration peak at 1,650 cm^{-1} in keratin shifts to 1,640 cm^{-1}

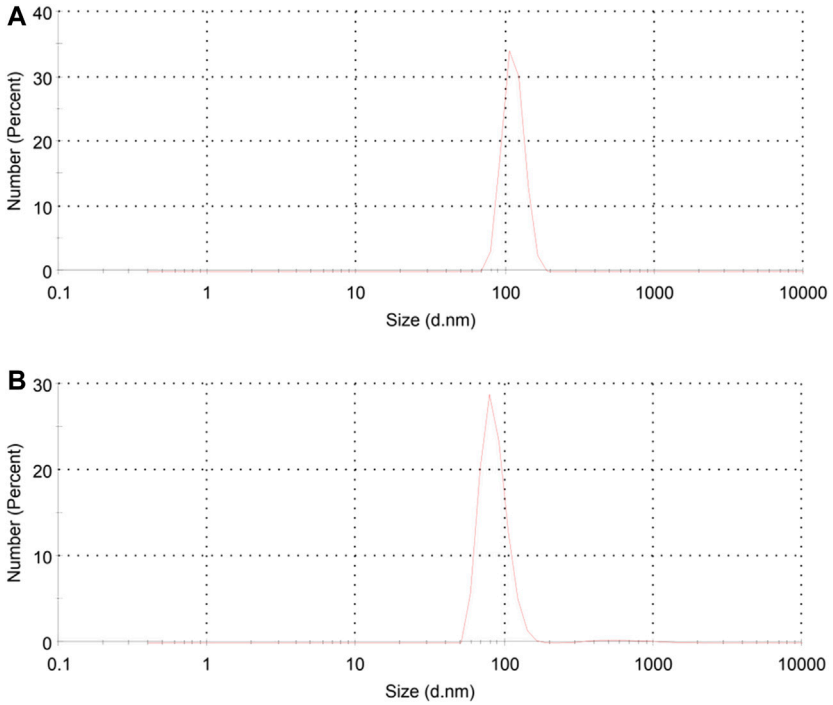

FIGURE 5 | Particle size distribution of **(A)** TGK21C5 and **(B)** TGK21C10.

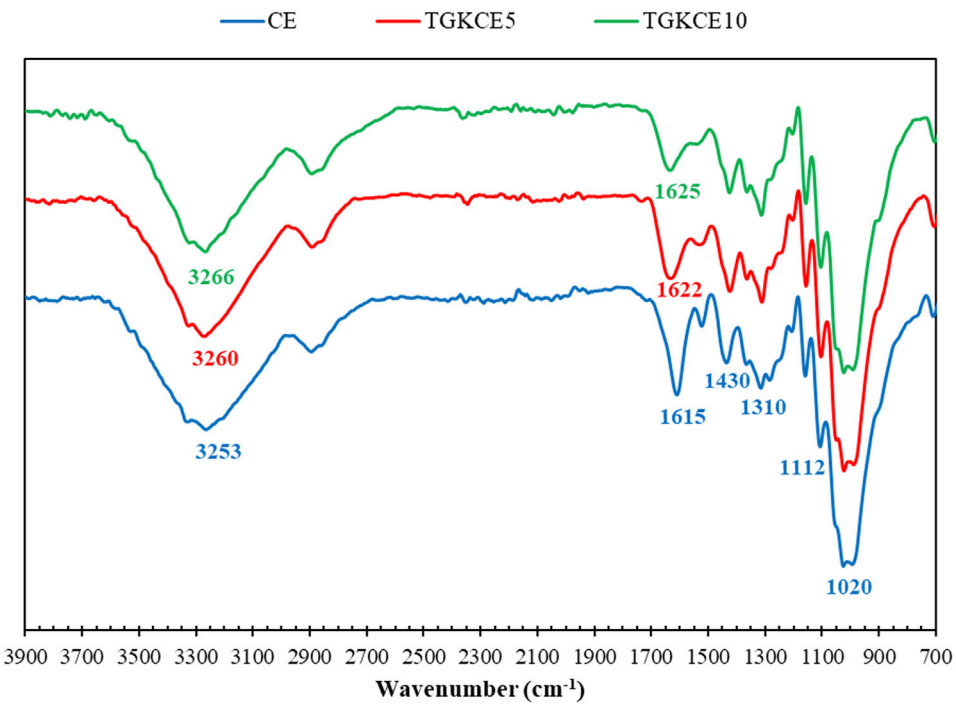

FIGURE 6 | FTIR spectra of pure CE and CE-loaded nanogels on cotton fabric.

in TGK composite. Further, the hydroxyl and carboxyl groups of TG could form hydrogen bonding with amine and carboxyl groups of keratin, which results in the broad peak in 3,000–3,700 cm^{-1} region.

XPS

XPS was employed to investigate the surface elemental composition of samples (**Figure 4**). The peaks with binding energy at 532, 400, and

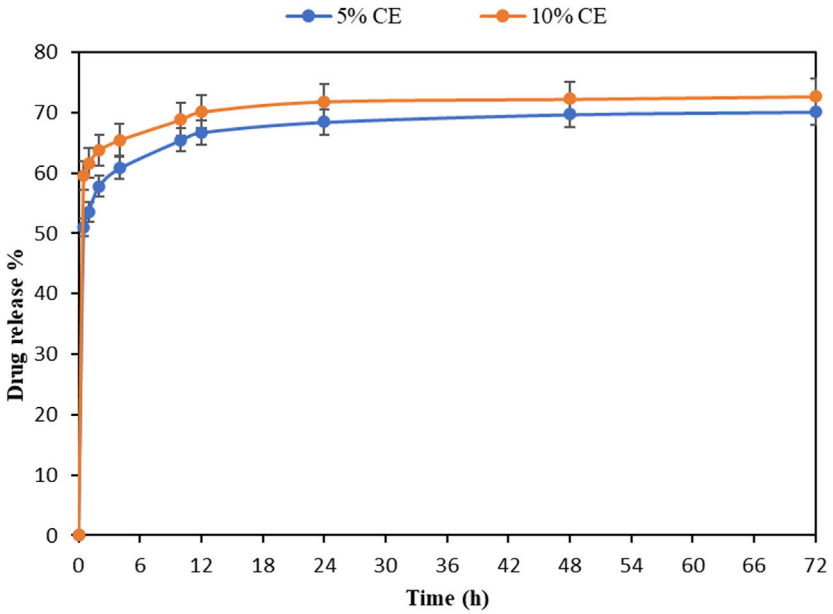

FIGURE 7 | Release profile of CE from treated cotton fabrics.

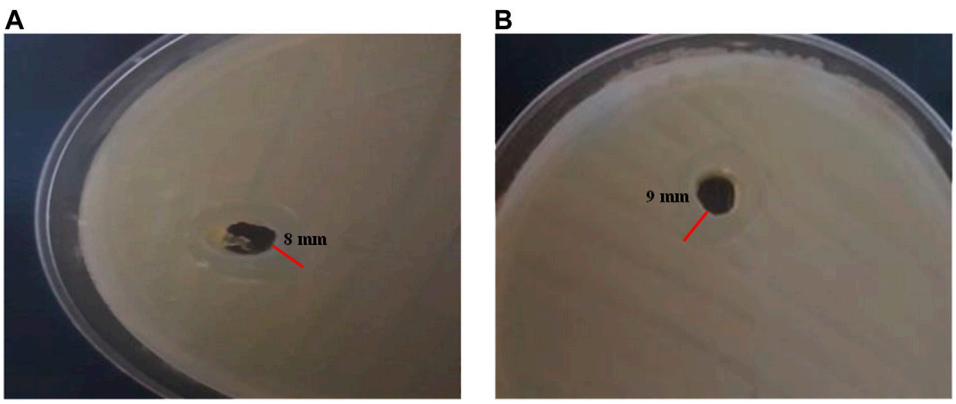

FIGURE 8 | Zone of inhibition against two bacteria: **(A)** *E. coli* and **(B)** *S. aureus*.

285 eV corresponding to oxygen (O1s), nitrogen (N1s), and carbon (C1s), respectively, represented the characteristic amino acid residues in keratin (**Figure 4A**). The distinctive elements of keratin presented in the spectra of TGK composite as well; however, the intensity of N content declined noticeably due to possible interactions of the employed polymers. An amide peak of ~288 eV (O=C–N) was observed in the high-resolution C1s region in keratin (**Figure 4B**), which was shifted to 286.1 eV in TGK. Besides, the peak at 285.8 eV (C-O, C-N) in keratin has been shifted to 284.4 (C-C, C-H) in TGK along with a decrease in the peak area (Kaur et al., 2018). In the S2p region (**Figure 4C**), a 163.6 eV peak was associated with the free thiols (-SH) in keratin (de Guzman et al., 2015). After cross-linking with H_2O_2, this peak was moved to 167.7 eV owing to the formation of disulfide bonds in TGK. It is worth mentioning that oxidative degradation of cystine disulfide S-S groups could lead to the formation of sulfur oxides -SO_3H (at ~168 eV) in keratin (Sun et al., 2017).

Characterization of CE-Loaded Nanogels

DLS

Figure 5 depicts the particle size distribution of CE-loaded TGK nanogels. The mean particle size of TGK21C5 and TGK21C10 was reported 85 and 105 nm, respectively. In comparison with the pristine TGK21 sample, it was found that the mean particles size increased after loading CE into the nanogels. The higher the amount of the extract, the bigger the sample size. This finding is in line with the study by Li et al. (2012) indicating an increase in the size of the produced nanoparticles after drug loading. It should be noted that both keratin and TG are natural macromolecules with various active groups on their molecule chain. These functional groups such as carboxyl, carbonyl, amine, and hydroxyl groups in TGK can interact

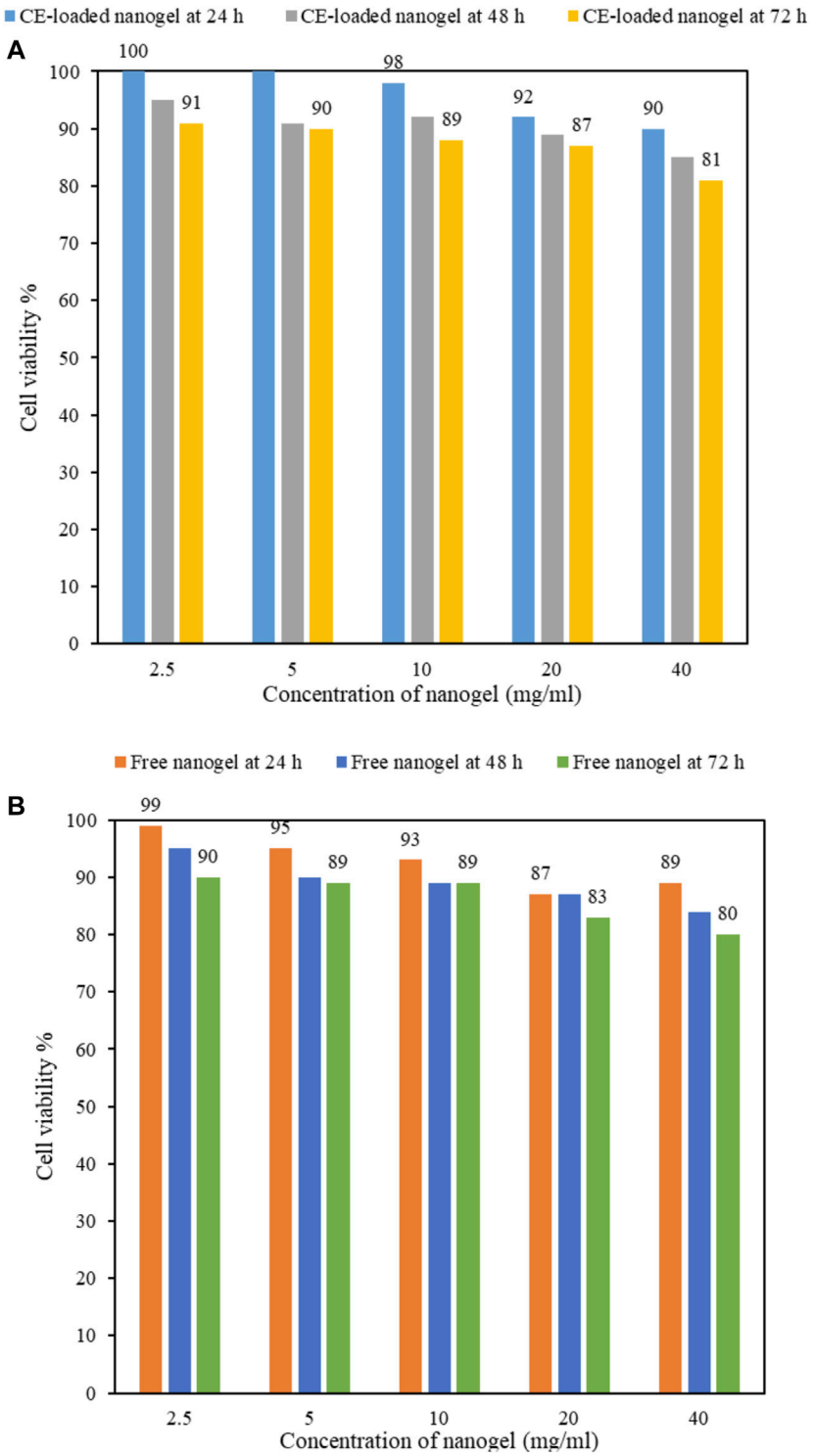

FIGURE 9 | Cell viability of nanogels **(A)** with and **(B)** without CE after 24, 48, and 72 h.

with the carbonyl and hydroxyl groups of CE *via* hydrogen bonding, which could stabilize the extract inside the nanogels leading to their growth in size. It is worth mentioning that the loading capacity of TGK nanogel was quantified by UVVis spectrophotometry, and the calculated CE loading content and encapsulation efficiency were approximately 62.7 and 42.3%, respectively. Similar results were reported by Sun et al. (2017) for keratin-alginate nanogel with enhanced drug loading efficiency.

FTIR

FTIR spectra of pure CE and CE-loaded nanogels on cotton fabrics are shown in **Figure 6**. The characteristic bands of CE exist at 1,020 cm^{-1} (deformation vibration of C-OH), 1,112 cm^{-1} (stretching vibration of C-O), 1,310 cm^{-1} (in-plane bending absorption of aromatic ring = C-H), 1,430 cm^{-1} (bending vibration of C-OH), 1,615 cm^{-1} (aromatic C=C stretching), and 3,253 cm^{-1} (O-H stretching) (Li et al., 2013; Boughendjioua et al., 2017). In the case of CE-loaded nanohydrogels, the characteristic peaks of cinnamon are vividly seen with slight movements. The peak shift from 1,615 cm^{-1} in CE to 1,622 cm^{-1} and 1,625 cm^{-1} in the nanogels loaded with 5 and 10% CE, respectively, might be owing to possible interactions between the components. The employed cotton fabric is a cellulosic-based polymer containing D-glucopyranose units linked with 1,4-glycosidic bonds. The cellulose chains are stacked together by van der Waals forces and strong intra- and/or intermolecular hydrogen bonds (Seddiqi et al., 2021). The possible hydrogen bonding between TGK, CE, and cellulose leads to the stabilization of the CE-loaded nanohydrogels on the cotton fabric.

Release Study

A good drug carrier should have the capacity to encapsulate drug molecules and release them under physiological condition sustainably (Sun et al., 2017). The release profile of encapsulated CE (5 and 10%) from treated fabrics is investigated in **Figure 7**. It can be seen that higher amount of CE was released with prolonging time, i.e., from 50 to 70% at 0.5 and 72 h for the sample containing 5% CE. Besides, more extract was released from the nanogels with higher amount of cinnamon, indicating that the release rate is related to the amount of the embedded extract. In the sample containing 10% CE, the release of about 73% occurred at the end, while in the sample containing 5% CE, 70% of CE was released at the same time point (72 h). The release curve shows a routine two-phase profile. The initial burst release may be related to the fast release of CE from the swollen nanogels, whereas the second phase (plateau after 12 h) is mainly associated with extract diffusion and hydrogel disruption. Due to the high anti-inflammatory property of the cinnamon extract (Gunawardena et al., 2015), the initial burst during the first 12 h will improve the efficiency of the nanohydrogels, especially at the first stage of wound healing. Previous studies have found that keratin-based nanogels can sustain the release of drugs and growth factors in correlation with their degradation (Li et al., 2012; Sun et al., 2017; Sun et al., 2018). In this study, as the release rate of the extract is concentration-dependent, it can be concluded that the observed release model follows the first-order kinetics model, which is in line with results obtained by Kumari and Sangal (2019). They found that the CE release from PLGA nanoparticles follows the first-order model.

Antibacterial Test

The antibacterial properties were assessed in agar medium for CE-loaded TGK nanogel against *E. coli* as a Gram-negative bacteria and *S. aureus* as a Gram-positive one. According to the obtained results in **Figure 8**, the zone of inhibition was calculated to be 9 mm for *S. aureus* and 8 mm for *E. coli*, indicating the suitable antibacterial activity of the extract in the fabricated nanogel. Literature review showed that the antibacterial activity of the CE was ascribed to the presence of cinnamaldehyde (Matan et al., 2006). It was reported that cinnamaldehyde can inhibit the production of an essential enzyme by the bacteria and disrupt the bacterial cell membrane (Helander et al., 1998; Firmino et al., 2018). Essential oils can inhibit bacterial growth activity and decrease the required active concentration of antibiotics by their synergistic activity (Sienkiewicz et al., 2014). It is worth mentioning that the L-sugars found in TG (i.e., L-arabinose and L-fucose) are responsible for the resistance to microbial attack because most organisms are unable to metabolize these foreign sugars (Ranjbar-Mohammadi and Bahrami, 2015).

Biocompatibility

The cytotoxicity of drug carriers is of great importance for their practical biomedical applications. MTT assay is one of the most commonly used colorimetric assay to evaluate cell viability through the determination of mitochondrial function of cells by measuring the activity of mitochondrial enzymes such as succinate dehydrogenase. In this assay, MTT is reduced to a purple formazan by NADH which is then quantified by its light absorbance (Aslantürk 2018). **Figure 9** exhibits the viability of nanogels with (**Figure 9A**) and without cinnamon (**Figure 9B**) at various concentrations (i.e., 2.5–40 mg/ml) using MTT assay on L929 fibroblast cells after different incubation times. As it can be seen in **Figure 9**, cell viability has decreased with increasing nanogels content, e.g., from 100 to 90% for 2.5 and 40 mg/ml CE-loaded nanogels at 24 h, respectively (**Figure 9A**); however, at all concentrations (even at relatively high concentrations up to 40 mg/ml), cell viability above 80% is obtained, implying the good biocompatibility of the fabricated TGK nanogels. This dose-dependent decrease in the viability was also studied by other researchers as well (Li et al., 2012). It is worth mentioning that both keratin and TG are biocompatible and biodegradable biopolymers that have been widely studied in biomedical applications. Keratin biomaterials have the capability to support cellular attachment and proliferation due to the presence of cell-binding motifs in the protein structure (Feroz et al., 2020). TG as a nonallergenic, nontoxic, and noncarcinogenic polysaccharide has also shown an improvement in the cell viability, attachment, and proliferation of fibroblast cells (Taghavizadeh Yazdi et al., 2021). As for cinnamon, Xie et al. (2018) reported that CE inhibited tumor cell proliferation in a dose-dependent manner. They found that anticancer properties of cinnamon were mediated by both downregulated their target cell cycle regulation molecules and mitosis regulation molecules.

As for the effect of time, with prolonging incubation time from 24 to 72 h, there is a reduction in cell viability in all the specimens, e.g., in 10 mg/ml free-nanogel from 93 to 89% at 24 and 72 h, respectively (**Figure 9B**). Moreover, an enhancement in cell viability was observed after cinnamon loading into the nanogels (e.g., at 24 h, from 93 to 98% for 10 mg/ml free-nanogel (**Figure 9B**) and CE-loaded nanogel (**Figure 9A**), respectively), owing to its high biological and antimicrobial properties (Sienkiewicz et al., 2014).

CONCLUSION

In this study, keratin was extracted from poultry feathers and mixed with TG to produce TGK nanogels at different ratios (keratin to TG: 1:1, 2:1, and 1:2). Then, CE (5 and 10%) was encapsulated into the nanogels, and the optimum sample was coated on cotton fabrics. DLS results showed an optimum sample size of approximately 80 nm for TGK21. According to TEM and FESEM images, spherical nanoparticles were formed. FTIR revealed possible interactions between the components in the composite. Moreover, the formation of disulfide bonds after cross-linking was confirmed by XPS. The mean size of the nanogel was increased from 80 to 85 and 105 nm after 5 and 10% loading of CE, respectively. The release profile of the extract from the treated fabrics was studied, and the results demonstrated a first-order release model. The antimicrobial test revealed that the incorporated extract showed proper antibacterial properties against both Gram-negative and Gram-positive bacteria. Results of MTT assay confirmed the biocompatibility of the nanogels indicating their potential applications in wound dressings and medical textiles.

DATA AVAILABILITY STATEMENT

The original contributions presented in the study are included in the article/supplementary material, further inquiries can be directed to the corresponding author.

AUTHOR CONTRIBUTIONS

NE contributed to conception and design of the study. NM performed experiments and analysis. NM and NE wrote the first draft of the manuscript. NE and AG-K performed data analysis. AG-K revised sections of the manuscript. All authors contributed to manuscript revision and approved the submitted version.

REFERENCES

Abdelhameed, R. M., Alzahrani, E., Shaltout, A. A., and Emam, H. E. (2021). Temperature-controlled-release of Essential Oil via Reusable Mesoporous Composite of Microcrystalline Cellulose and Zeolitic Imidazole Frameworks. *J. Ind. Eng. Chem.* 94, 134–144. doi:10.1016/j.jiec.2020.10.025

Amin, S., Rajabnezhad, S., and Kohli, K. (2009). Hydrogels as Potential Drug Delivery Systems. *Sci. Res. Essays.* 4, 1175–1183. doi:10.5897/SRE.9000559

Aslantürk, Ö. S. (2018). "*In Vitro* cytotoxicity and Cell Viability Assays: Principles, Advantages, and Disadvantages," in *Genotoxicity-A Predictable Risk to Our Actual World*, 64–80. doi:10.5772/intechopen.71923

Boughendjioua, H., Amoura, N., and Boughendjioua, Z. (2017). Purity Specifications of Constituents of Cinnamon Essential Oil by Fourier Transformed Infrared Spectroscopy Analysis. *Ijpbr* 5, 36–40. doi:10.30750/ijpbr.5.2.7

Chacko, R. T., Ventura, J., Zhuang, J., and Thayumanavan, S. (2012). Polymer Nanogels: A Versatile Nanoscopic Drug Delivery Platform. *Adv. Drug Deliv. Rev.* 64, 836–851. doi:10.1016/j.addr.2012.02.002

Cheng, R., Meng, F., Deng, C., Klok, H.-A., and Zhong, Z. (2013). Dual and Multi-Stimuli Responsive Polymeric Nanoparticles for Programmed Site-specific Drug Delivery. *Biomaterials* 34, 3647–3657. doi:10.1016/j.biomaterials.2013.01.084

Cheng, Z., Chen, X., Zhai, D., Gao, F., Guo, T., Li, W., et al. (2018). Development of Keratin Nanoparticles for Controlled Gastric Mucoadhesion and Drug Release. *J. Nanobiotechnol.* 16, 24. doi:10.1186/s12951-018-0353-2

Cilurzo, F., Selmin, F., Aluigi, A., and Bellosta, S. (2013). Regenerated Keratin Proteins as Potential Biomaterial for Drug Delivery. *Polym. Adv. Technol.* 24, 1025–1028. doi:10.1002/pat.3168

de Guzman, R. C., Tsuda, S. M., Ton, M.-T. N., Zhang, X., Esker, A. R., and Van Dyke, M. E. (2015). Binding Interactions of Keratin-Based Hair Fiber Extract to Gold, Keratin, and BMP-2. *PLoS One* 10, e0137233. doi:10.1371/journal.pone.0137233

Debalke, D., Birhan, M., Kinubeh, A., and Yayeh, M. (2018). Assessments of Antibacterial Effects of Aqueous-Ethanolic Extracts of Sida Rhombifolia's Aerial Part. *Scientific World J.* 2018, 1–8. doi:10.1155/2018/8429809

Emam, H. E., Darwesh, O. M., and Abdelhameed, R. M. (2020). Protective Cotton Textiles via Amalgamation of Cross-Linked Zeolitic Imidazole Frameworks. *Ind. Eng. Chem. Res.* 59, 10931–10944. doi:10.1021/acs.iecr.0c01384

Eslahi, N., Dadashian, F., and Nejad, N. H. (2013). An Investigation on Keratin Extraction from Wool and Feather Waste by Enzymatic Hydrolysis. *Prep. Biochem. Biotechnol.* 43, 624–648. doi:10.1080/10826068.2013.763826

Fattahi, A., Petrini, P., Munarin, F., Shokoohinia, Y., Golozar, M. A., Varshosaz, J., et al. (2013). Polysaccharides Derived from Tragacanth as Biocompatible Polymers and Gels. *J. Appl. Polym. Sci.* 129, 2092–2102. doi:10.1002/app.38931

Feroz, S., Muhammad, N., Ratnayake, J., and Dias, G. (2020). Keratin - Based Materials for Biomedical Applications. *Bioactive Mater.* 5, 496–509. doi:10.1016/j.bioactmat.2020.04.007

Firmino, D. F., Cavalcante, T. T. A., Gomes, G. A., Firmino, N. C. S., Rosa, L. D., de Carvalho, M. G., et al. (2018). Antibacterial and Antibiofilm Activities of Cinnamomum Sp. Essential Oil and Cinnamaldehyde: Antimicrobial Activities. *Scientific World J.* 2018, 1–9. doi:10.1155/2018/7405736

Ghayempour, S., Montazer, M., and Mahmoudi Rad, M. (2016). Encapsulation of Aloe Vera Extract into Natural Tragacanth Gum as a Novel green Wound Healing Product. *Int. J. Biol. Macromolecules* 93, 344–349. doi:10.1016/j.ijbiomac.2016.08.076

Gunawardena, D., Karunaweera, N., Lee, S., van Der Kooy, F., Harman, D. G., Raju, R., et al. (2015). Anti-inflammatory Activity of Cinnamon (C. Zeylanicum and C. cassia) Extracts - Identification of E-Cinnamaldehyde and O-Methoxy Cinnamaldehyde as the Most Potent Bioactive Compounds. *Food Funct.* 6, 910–919. doi:10.1039/c4fo00680a

Helander, I. M., Alakomi, H.-L., Latva-Kala, K., Mattila-Sandholm, T., Pol, I., Smid, E. J., et al. (1998). Characterization of the Action of Selected Essential Oil Components on Gram-Negative Bacteria. *J. Agric. Food Chem.* 46, 3590–3595. doi:10.1021/jf980154m

Kaur, M., Arshad, M., and Ullah, A. (2018). *In-Situ* Nanoreinforced Green Bionanomaterials from Natural Keratin and Montmorillonite (MMT)/Cellulose Nanocrystals (CNC). *ACS Sust. Chem. Eng.* 6, 1977–1987. doi:10.1021/acssuschemeng.7b03380

Kumari, V., and Sangal, A. (2019). Synthesis, Characterization, Antimicrobial Activity and Release Study of Cinnamon Loaded Poly (DL-Lactide-Co-Glycolide) Nanoparticles. *Rese. Jour. Pharm. Technol.* 12, 1529. doi:10.5958/0974-360X.2019.00253.1

Kwon, H.-K., Hwang, J.-S., So, J.-S., Lee, C.-G., Sahoo, A., Ryu, J.-H., et al. (2010). Cinnamon Extract Induces Tumor Cell Death through Inhibition of NFκB and AP1. *BMC Cancer* 10, 392. doi:10.1186/1471-2407-10-392

Li, Q., Zhu, L., Liu, R., Huang, D., Jin, X., Che, N., et al. (2012). Biological Stimuli Responsive Drug Carriers Based on Keratin for Triggerable Drug Delivery. *J. Mater. Chem.* 22, 19964–19973. doi:10.1039/C2JM34136K

Li, Y.-q., Kong, D.-x., and Wu, H. (2013). Analysis and Evaluation of Essential Oil Components of Cinnamon Barks Using GC-MS and FTIR Spectroscopy. *Ind. Crops Prod.* 41, 269–278. doi:10.1016/j.indcrop.2012.04.056

Matan, N., Rimkeeree, H., Mawson, A. J., Chompreeda, P., Haruthaithanasan, V., and Parker, M. (2006). Antimicrobial Activity of Cinnamon and Clove Oils under Modified Atmosphere Conditions. *Int. J. Food Microbiol.* 107, 180–185. doi:10.1016/j.ijfoodmicro.2005.07.007

McKenzie, M., BettsSuh, D. A., Suh, A., Bui, K., Kim, L., and Cho, H. (2015). Hydrogel-Based Drug Delivery Systems for Poorly Water-Soluble Drugs. *Molecules* 20, 20397–20408. doi:10.3390/molecules201119705

Meghdadi, K. R., and Boddohi, S. (2019). Preparation and Investigation of Gum Tragacanth/Gelatin Nanofibers for Antibacterial Drug Delivery Systems. Iran. *J. Polym. Sci. Technol. (Persian Ed.* 32, 145–155. doi:10.22063/JIPST.2019.1650

Nazarzadeh Zare, E., Makvandi, P., and Tay, F. R. (2019). Recent Progress in the Industrial and Biomedical Applications of Tragacanth Gum: A Review. *Carbohydr. Polym.* 212, 450–467. doi:10.1016/j.carbpol.2019.02.076

Pathania, D., Verma, C., Negi, P., Tyagi, I., Asif, M., Kumar, N. S., et al. (2018). Novel Nanohydrogel Based on Itaconic Acid Grafted Tragacanth Gum for Controlled Release of Ampicillin. *Carbohydr. Polym.* 196, 262–271. doi:10.1016/j.carbpol.2018.05.040

Ranjbar-Mohammadi, M., and Bahrami, S. H. (2015). Development of Nanofibrous Scaffolds Containing Gum Tragacanth/poly (ε-Caprolactone) for Application as Skin Scaffolds. *Mater. Sci. Eng. C.* 48, 71–79. doi:10.1016/j.msec.2014.10.020

Seddiqi, H., Oliaei, E., Honarkar, H., Jin, J., Geonzon, L. C., Bacabac, R. G., et al. (2021). Cellulose and its Derivatives: towards Biomedical Applications. *Cellulose* 28, 1893–1931. doi:10.1007/s10570-020-03674-w

Sienkiewicz, M., Głowacka, A., Kowalczyk, E., Wiktorowska-Owczarek, A., Jóźwiak-Bębenista, M., and Łysakowska, M. (2014). The Biological Activities of Cinnamon, Geranium and Lavender Essential Oils. *Molecules* 19, 20929–20940. doi:10.3390/molecules191220929

Singh, B., and Sharma, V. (2014). Influence of Polymer Network Parameters of Tragacanth Gum-Based pH Responsive Hydrogels on Drug Delivery. *Carbohydr. Polym.* 101, 928–940. doi:10.1016/j.carbpol.2013.10.022

Sun, Z., Yi, Z., Cui, X., Chen, X., Su, W., Ren, X., et al. (2018). Tumor-targeted and Nitric Oxide-Generated Nanogels of Keratin and Hyaluronan for Enhanced Cancer Therapy. *Nanoscale* 10, 12109–12122. doi:10.1039/C8NR03265C

Sun, Z., Yi, Z., Zhang, H., Ma, X., Su, W., Sun, X., et al. (2017). Bio-responsive Alginate-Keratin Composite Nanogels with Enhanced Drug Loading Efficiency for Cancer Therapy. *Carbohydr. Polym.* 175, 159–169. doi:10.1016/j.carbpol.2017.07.078

Taghavizadeh Yazdi, M. E., Nazarnezhad, S., Mousavi, S. H., Sadegh Amiri, M., Darroudi, M., Baino, F., et al. (2021). Gum Tragacanth (GT): A Versatile Biocompatible Material beyond Borders. *Molecules* 26, 1510. doi:10.3390/molecules26061510

Verma, C., Negi, P., Pathania, D., Anjum, S., and Gupta, B. (2020). Novel Tragacanth Gum-Entrapped Lecithin Nanogels for Anticancer Drug Delivery. *Int. J. Polymeric Mater. Polymeric Biomater.* 69, 604–609. doi:10.1080/00914037.2019.1596910

Xie, G. Y., Ma, J., Guan, L., Liu, X. M., Wang, A., and Hu, C. H. (2018). Proliferation Effects of Cinnamon Extract on Human Hela and HL-60 Tumor Cell Lines. *Eur. Rev. Med. Pharmacol. Sci.* 22, 5347–5354. doi:10.26355/eurrev_201808_15736

Zhang, H., and Liu, P. (2019). One-Pot Synthesis of Chicken-Feather-Keratin-Based Prodrug Nanoparticles with High Drug Content for Tumor Intracellular DOX Delivery. *Langmuir* 35, 8007–8014. doi:10.1021/acs.langmuir.9b01190

Conflict of Interest: The authors declare that the research was conducted in the absence of any commercial or financial relationships that could be construed as a potential conflict of interest.

Publisher's Note: All claims expressed in this article are solely those of the authors and do not necessarily represent those of their affiliated organizations, or those of the publisher, the editors and the reviewers. Any product that may be evaluated in this article, or claim that may be made by its manufacturer, is not guaranteed or endorsed by the publisher.